

Li, R, Shi, X, Sheng, Y and Zhang, G

**A new area-based convexity measure with distance weighted area integration for planar shapes**

<http://researchonline.ljmu.ac.uk/id/eprint/10645/>

#### Article

**Citation** (please note it is advisable to refer to the publisher's version if you intend to cite from this work)

**Li, R, Shi, X, Sheng, Y and Zhang, G (2019) A new area-based convexity measure with distance weighted area integration for planar shapes. Computer Aided Geometric Design (A GMP'19 paper), 71. pp. 176-189. ISSN 0167-8396**

LJMU has developed [LJMU Research Online](http://researchonline.ljmu.ac.uk/) for users to access the research output of the University more effectively. Copyright © and Moral Rights for the papers on this site are retained by the individual authors and/or other copyright owners. Users may download and/or print one copy of any article(s) in LJMU Research Online to facilitate their private study or for non-commercial research. You may not engage in further distribution of the material or use it for any profit-making activities or any commercial gain.

The version presented here may differ from the published version or from the version of the record. Please see the repository URL above for details on accessing the published version and note that access may require a subscription.

For more information please contact [researchonline@ljmu.ac.uk](mailto:researchonline@ljmu.ac.uk)

# A New Area-based Convexity Measure with Distance Weighted Area Integration for Planar Shapes

Rui Li<sup>a,b</sup>, Xiayan Shi<sup>a,b</sup>, Yun Sheng<sup>c,\*</sup>, Guixu Zhang<sup>a,b</sup>

<sup>a</sup>Shanghai Key Laboratory of Multidimensional Information Processing, East China Normal University, Shanghai, People's Republic of China

<sup>b</sup>The Department of Computer Science and Technology, East China Normal University, Shanghai, People's Republic of China

<sup>c</sup>The Department of Computer Science, Liverpool John Moores University, L3 3AF, UK

---

## Abstract

In this paper we propose a new area-based convexity measure. We assume that convexity evaluation of an arbitrary planar shape is related to the total influence of dents of the shape, and discover that those attributes of the dents, such as the position, area, and depth with respect to the Geometric Center of Convex Hull (GCCH) of the shape, determine the dent influence. We consider that the convex hull of the shape consists of infinitely small patches, to each of which we assign a weight showing the patch influence. We can simply integrate all the patch weights in any regions within the convex hull to calculate their total influence. We define this operation as the Distance Weighted Area Integration, if the weight is associated with the Euclidean distance from the patch to the GCCH. Our new measure is a distance weighted generalization of the most commonly used convexity measure, making this conventional measure fully replaceable for the first time. Experiments demonstrate advantages of the new convexity measure against the existing ones.

*Keywords:* Shape analysis, shape representation, convexity

---

## 1. Introduction

Shape is a common feature extensively used by human beings to perceive, study, recognize, describe, and represent the visual world, while convexity is a holistic scalar widely adopted to describe and represent geometric shapes. In practice, shape representation is hampered from time to time by shape position, size, orientation as well as noise. To this end, a shape descriptor robust enough against translation, scaling, rotation, and noise is desired. Traditionally, 2D shape representation algorithms can be classified into space domain methods and scalar transform methods [Loncaric \(1998\)](#): The former map shapes into space domains, such as graphs and images, and typical examples of the space domain methods involve chain code and medial axis transform, *etc.*; the latter convert shapes into scalars or vectors in a numeric fashion, for example Fourier descriptors and moments, *etc.* There exist some scalar transform methods that describe and measure geometric shapes in a neat and holistic manner with only one scalar value. These methods, which are also learning-free, when employed in applications such as shape retrieval and classification, are computationally more efficient than learning-based methods as well as those requiring extra operations such as pose registration, feature correspondence, or model fitting. The holistic scalars commonly used to describe and measure geometric shapes involve compactness [Bribiesca \(2008\)](#); [Zunic et al. \(2010\)](#), rectangularity [Rosin \(1999, 2003\)](#), ellipticity [Proffitt \(1982\)](#), rectilinearity [Lian et al. \(2010\)](#); [Zunic and Rosin \(2003\)](#), concavity [Lien and Amato \(2006\)](#), convexity [Lian et al. \(2012\)](#); [Rahtu et al. \(2006\)](#), and so on. Among

---

\*Corresponding author

Email addresses: [lirui123456@qq.com](mailto:lirui123456@qq.com) (Rui Li), [913810856@qq.com](mailto:913810856@qq.com) (Xiayan Shi), [y.sheng@ljmu.ac.uk](mailto:y.sheng@ljmu.ac.uk) (Yun Sheng), [gxzhang@cs.ecnu.edu.cn](mailto:gxzhang@cs.ecnu.edu.cn) (Guixu Zhang)

them convexity has been most widely studied and used in classification [Rahtu et al. \(2006\)](#); [Zunic and Rosin \(2004\)](#); [Rosin \(2009\)](#), retrieval [Lian et al. \(2012\)](#); [Li et al. \(2017\)](#), non-photorealistic rendering [Song et al. \(2013\)](#), figure/ground separation [Pao et al. \(1999\)](#), and shape decomposition [Asafi et al. \(2013\)](#); [Ghosh et al. \(2013\)](#); [Liu et al. \(2010\)](#); [Zhou et al. \(2013\)](#); [Lien and Amato \(2007\)](#); [Attene et al. \(2008\)](#).

Current mainstream 2D convexity measures can be divided into three categories: Boundary-based [Zunic and Rosin \(2004\)](#), probability-based [Rahtu et al. \(2006\)](#); [Rosin and Zunic \(2007\)](#), and area-based [Rosin and Mumford \(2006\)](#) convexity measures. In general a planar shape  $S$  is considered as convex if and only if the line segment between any two points in  $S$  belongs to  $S$ . This notion of convexity can be easily used to derive some probability-based measures, and these probability-based measures may characterize either area-based [Rahtu et al. \(2006\)](#) or boundary-based measures [Rosin and Zunic \(2007\)](#). However, the probability-based measures may suffer from computational infeasibility or range shrinkage of the convexity value. The boundary-based measures suitable for applications that need a strong response to slight shape changes are sensitive to noise and insensitive to dent translation [Rosin and Zunic \(2007\)](#). The area-based measures are robust against noise and can be used in classification of noise distorted shapes. Due to its computational simplicity and robustness against noise, the most commonly used measure is an area-based measure [Zunic and Rosin \(2004\)](#), which defines the convexity of a planar shape as a ratio of shape area to its convex hull area. Nevertheless, this area-based measure is insensitive to dent translation and rotation. Although another area-based convexity measure has been proposed afterwards [Rosin and Mumford \(2006\)](#), it cannot eradicate the above problems of the most commonly used measure. Note that previous research has shown that a well-defined convexity measure should be sensitive to shapes with dents under affine transformations such as translation and rotation [Zunic and Rosin \(2004\)](#); [Rosin and Zunic \(2007\)](#). Therefore, being sensitive to dent translation and rotation is a key criterion to evaluation of the convexity measures in this paper.

In this paper we bridge the above technical gaps by presenting a new area-based convexity measure, which is built on the most commonly used one but excels it by resolving its extant problems for planar shapes. Moreover, the new measure robust against shape translation, scaling, rotation as well as noise may offer a holistic and efficient way for applications where shape representation is required. Our new measure is based on the following assumptions and easy to understand. We assume that dents of an arbitrary nonconvex shape are formed by region collapsing from its convex hull, and observe that those attributes of dents, such as the position, area, and depth with respect to the geometric center of convex hull of the shape, influence the computation of convexity. Therefore, the philosophy behind our convexity measure is that the convexity of an arbitrary planar shape is computed by subtracting the total influence of all the dents from that of the convex hull of the shape, and then by dividing the subtracted result by the whole influence of convex hull of the shape for normalization. Moreover, the influence of dents is evaluated in association with the aforementioned dent attributes. Generally, the less the influence of their dents, the more convex the shape. For a completely convex shape the influence of its dents is apparently null and its convexity thus reaches the maximum. This paper is dedicated to an implementation of the above analysis based on a notion named the Distance Weighted Area Integration (DWAI) for influence evaluation. The major contributions of this paper are summarized as follows:

1. For the first time have we ameliorated the most commonly used convexity measure by turning it into a problem of influence evaluation through the DWAI, making it fully replaceable.
2. We have mathematically showed the connections of our new measure to the most commonly used by deducing some new properties.
3. Experiments have showed that the new measure has advantages over the mainstream competitors in many aspects.

Before we review some typical convexity measures that can sufficiently represent the current state of the art, it must be clarified that there are four properties that every convexity measure must hold:

1. the convexity measure is a number between  $(0,1]$ ;
2. the convexity measure of a given shape equals 1 if and only if this shape is convex;
3. there are shapes whose convexity measure is arbitrary close to 0;
4. the convexity measure of a shape is invariant under similarity transformations of this shape.

## 2. Related work

We start this section by looking at a simple definition of boundary-based convexity measurement below.

**Definition 1.** For a given planar shape  $S$ , its convexity is measured as

$$C_1(S) = \frac{Per_2(CH(S))}{Per_2(S)}, \quad (1)$$

where  $CH(S)$  indicates the convex hull of  $S$ ,  $Per_2(CH(S))$  and  $Per_2(S)$  are the Euclidean perimeters of  $CH(S)$  and  $S$ , respectively.

$C_1$  is insensitive to dent rotation within the convex hull of the shape. To address this issue Zunic *et al.* presented an improved boundary-based convexity measure with the idea of boundary projection Zunic and Rosin (2004):

**Definition 2.** For a given planar shape  $S$ , its convexity is measured as

$$C_2(S) = \min_{\varphi \in [0, 2\pi]} \frac{Per_2(R(S, \varphi))}{Per_1(S, \varphi)}, \quad (2)$$

where  $Per_1(S)$  is perimeter of  $S$  calculated in Manhattan distance.  $R(S, \varphi)$  denotes the minimal bounding rectangle with its edges parallel to the coordinate axes, where  $S$  is rotated around the origin by an angle  $\varphi$ .

As reviewed previously, the boundary-based methods are sensitive to noise and insensitive to dent translation. Some convexity measures make use of probabilistic interpretation. For example,  $C_3$  is defined as the probability that for any randomly chosen points  $X$  and  $Y$  from  $S$  all points on the line segment  $[X, Y]$  also belong to  $S$ , under the assumption that  $X$  and  $Y$  are chosen uniformly.

**Definition 3.** For a given planar shape  $S$ , its convexity is measured as  $C_3(S) = P([X, Y] \in S)$

In practice,  $C_3$  is difficult to compute, even if  $S$  is a polygon Zunic and Rosin (2004). To this problem, Rahtu *et al.* Rahtu *et al.* (2006) improved this measure by using point probability rather than line segment probability. Their measure  $C_\alpha$  is defined as the probability of a point belonging to a line segment  $[X, Y]$ :

**Definition 4.** For a given planar shape  $S$ , its convexity is measured as  $C_\alpha(S) = P(\alpha X + (1 - \alpha)Y \in S)$ , where  $\alpha$  determines the location of the point on the line segment with  $0 < \alpha < 1$ .

Since evaluating  $C_\alpha$  by sampling is impractical, Rahtu *et al.* have proposed to calculate  $C_\alpha$  with the Fourier transform. This approximation with the Fourier transform makes the convexity value calculated by  $C_\alpha$  unreasonably higher than expected, and such examples of  $C_\alpha$  can be found in Fig.12. Moreover,  $C_\alpha$  is insensitive of slim protrusions, as shown in Fig.11.

Due to computational simplicity and robustness against noise, the most commonly used measure defines the convexity of a planar shape as a ratio of shape area to its convex hull area Zunic and Rosin (2004).

**Definition 5.** For a given planar shape  $S$ , its convexity based on the area can be measured as

$$C_4(S) = \frac{Area(S)}{Area(CH(S))}. \quad (3)$$

$C_4$  only considers the area of  $S$  and  $CH(S)$ , and its ratio cannot precisely represent the real convexity. For example, in Fig.1 shape  $S_2$  is perceptually more concave than  $S_1$ . However, the convexities of  $S_1$  and  $S_2$  calculated by  $C_4$  are 0.9620 and 0.9714.

Another area-based convexity measure is defined as the ratio of the area of  $MCS(S)$  to that of the original shape  $S$ , where  $MCS(S)$  denotes a convex subset of  $S$  with the maximum area:

**Definition 6.** For a given planar shape  $S$ , its convexity can be measured as

$$C_5(S) = \frac{Area(MCS(S))}{Area(S)}. \quad (4)$$

Since  $MCS(S)$  is difficult to calculate,  $C_5$  has been rarely used in practical applications.

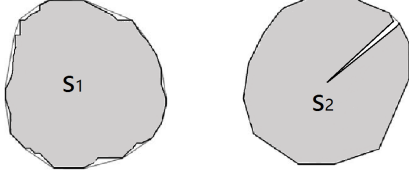


Figure 1: An unreasonable example of  $C_4$ .

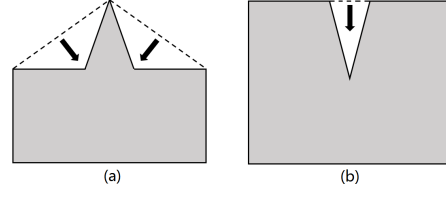


Figure 2: (a) and (b) are two nonconvex shapes. Shape (a) can be thought of as a combination of a rectangle with a protrusion part while Shape (b) as a rectangle with a dent. We can regard both of the shapes as collapsed from their convex hulls, with the black arrows implying the collapsing directions.

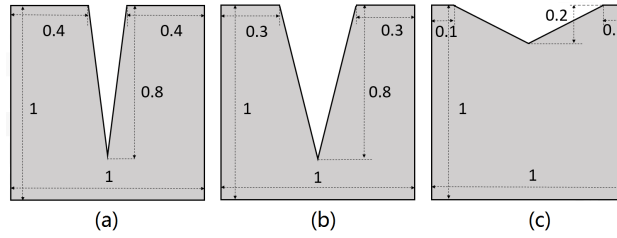


Figure 3: The depth values of the dents in Shape (a) and (b) are equal and the areas of the dents in Shape (a) and (c) are equal.

### 3. A new convexity measure

We start the new convexity measurement by defining two concepts repeatedly mentioned in the paper.

**GCCH:** For a given planar shape  $S$ , its geometric center is the arithmetic mean position of all the points in  $S$ . Similarly, the Geometric Center of its Convex Hull  $CH(S)$  of  $S$  is the arithmetic mean position of all the points in  $CH(S)$ . As the term, Geometric Center of Convex Hull of the shape, is frequently referred in this paper, we instead adopt its abbreviation GCCH for the sake of simplicity.

**DWAI:** For a given planar shape  $S$ , all the points in  $S$  can be weighted in some way. The integration of all the weighted points is defined as the Weighted Area Integration (WAI). In this paper a way called the Distance Weighted Area Integration (DWAI) is used to weight all the points in the planar shape with respect to their Euclidean distance to the GCCH.

#### 3.1. Analysis

The new convexity measure is based on an intuitive observation that any planar nonconvex shape  $S$ , no matter with a protrusion or dent, as shown in Fig.2, can be regarded as collapsed from its convex hull. Thus, we assume that the convexity computation of an arbitrary shape is related to the total influence of dents collapsed from the convex hull of the shape, and consider that those attributes of dents, such as the position, area, and depth with respect to the GCCH of the shape, directly decide the influence of dents.

Some intuitional examples are given in Fig.3. In Fig.3, it can be observed that (b) is lower in convexity than (a). This distinction cannot be sensed by  $C_2$ . The convexities of Shape (a) and (b) computed by  $C_2$  are both 0.714, while the convexities of Shape (a) and (b) computed by  $C_1$  are 0.739 and 0.762, also a negative example. It is also observed that (a) is lower in convexity than (c). However, the convexities of (a) and (c) computed by  $C_4$  hold the same value 0.920, and thus fail to reflect the difference. Similarly, although the dent, as it moves in Fig.7 (a), remains identical in area and depth, it influences the shape variably.  $C_5$  and  $C_\alpha$  can sense this distinction while  $C_1$ ,  $C_2$ , and  $C_4$  not. As suggested above, all the position, area, and depth of dents with respect to the GCCH of the shape will influence the convexity measurement.

### 3.2. Definition of the new convexity measure

We assume that the convex hull of a shape consists of infinitely small patches and every patch has an influence on and contributes to the calculation of convexity. Note that in this case the infinitely small patch is the equivalent of a point or a discrete pixel in a digital image. We assign each patch a weight associated with the Euclidean distance from the patch to the GCCH to measure the patch influence. The closer a patch to the GCCH, the more it contributes to the convexity. For example, there are many dents on the boundary of  $S_1$  in Fig.1, but these dents impose little influence on the shape. Therefore, the total influence of dents  $I(D)$  can be measured by the WAI as  $\iint_D W(r)d\sigma$ , where  $D$  symbolizes the region that dents cover, and  $W(r)$  is the integrand indicating the weight of each infinitely small patch,  $d\sigma$ . The influence of shape  $S$ ,  $I(S)$ , is the result of subtracting  $I(D)$  from that of its convex hull,  $I(CH(S))$ , which can be written in terms of WAI as  $\iint_{CH(S)} W(r)d\sigma - \iint_D W(r)d\sigma$ , and can be rewritten as  $\iint_S W(r)d\sigma$  for simplicity. In order to confine the result to  $(0, 1]$ , we divide  $I(S)$  by  $I(CH(S))$  for normalization.

**Definition 7.** For a given planar shape  $S$ , its convexity measure  $C_\beta$  is defined as

$$C_\beta(S) = \frac{I(S)}{I(CH(S))} = \frac{\iint_S W(r)d\sigma}{\iint_{CH(S)} W(r)d\sigma}, \quad (5)$$

where

$$W(r) = 1 - \beta \cdot \frac{r}{r_{\max}}, \quad (6)$$

with  $0 \leq \beta \leq 1$ .  $r$  represents the Euclidean distance between a patch and the GCCH; and  $r_{\max}$  is the maximum one of all  $r$ s.

Eq.(5) and (6) explains our notion of the DWAI. When  $r = r_{\max}$ , we have a minimal weight,  $1 - \beta$ . When  $r = 0$ , we have a maximum weight, 1. Therefore, the range of  $W(r)$  is  $[1 - \beta, 1]$ . By adjusting  $\beta$  we can control the influence of different attributes. For example, if we want to emphasize the influence of the dent position, we can increase  $\beta$  to lower the weights of distant patches. If we want to emphasize the influence of the dent area, we can decrease the value of  $\beta$  to degrade the weight influence of each patch. For example, when we decrease  $\beta$  to 0, every patch will have an identical weight, and the new measure will degenerate into the traditional area-based convexity measure  $C_4$ , the measurement of which only depends on the dent area. Generally, the form of  $W(r)$  is versatile enough to be explored. We make it open for further study here.

The following theorem summarizes the four desirable properties that every convexity measure must hold.

**Theorem 1.** For a given planar shape  $S$ ,

1.  $0 < C_\beta(S) \leq 1$ ;
2.  $C_\beta(S) = 1$  if and only if  $S$  is convex;
3.  $\inf_{S \in \Pi} (C_\beta(S)) = 0$ , where  $\Pi$  denotes the set of all planar shapes;
4.  $C_\beta(S)$  is invariant under similarity transformations.

*Proof.* For a given planar shape  $S$ , assume that it has  $n$  dents denoted as  $D_1, D_2, \dots, D_n$ . The corresponding influences of dents  $D_1, D_2, \dots, D_n$  are  $\iint_{D_1} W(r)d\sigma, \iint_{D_2} W(r)d\sigma, \dots, \iint_{D_n} W(r)d\sigma$ , respectively, and can be simplified as  $I(D_1), I(D_2), \dots, I(D_n)$ . Thus,  $C_\beta(S)$  can be rewritten as

$$C_\beta(S) = \frac{I(S)}{I(S) + \sum_{j=1}^n I(D_j)}. \quad (7)$$

It is easy to show that  $0 < C_\beta(S) < 1$ . If there is no dent, that is  $\sum_{j=1}^n I(D_j) = 0$ , then  $C_\beta(S) = 1$ . This means that  $S$  coincides with its convex hull. To this end,  $S$  is convex. For a toroidal shape in Fig.4, if the value

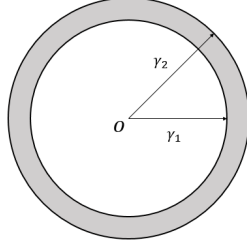


Figure 4: Shape  $S$  is a torus and its inner radius and outer radius are  $\gamma_1$  and  $\gamma_2$ , respectively.

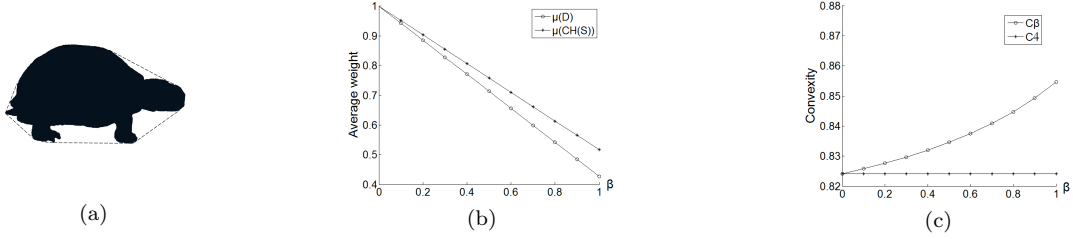


Figure 5: The dents in (a) are relatively distant from the GCCH of the shape. According to Properties 2 and 3, increasing  $\beta$  will enlarge the difference between  $\mu(D)$  and  $\mu(CH(S))$  and increase the value of  $C_\beta$ .

of  $\gamma_2 - \gamma_1$  tends to be infinitesimally small, and the area of  $S$  also approaches 0, then  $I(S)$  will approach 0, that is  $\lim_{\gamma_2 - \gamma_1 \rightarrow 0} C_\beta(S) = 0$ .

For translation and rotation of the shape, because the relevant distance between each patch and the GCCH remains the same, and the size of the shape and dents remains unchanged, the convexity remains the same. When the shape is scaled, the distance between each patch and the GCCH changes. Taking the GCCH as the origin to establish the coordinate system, we can compute the convexity before the scaling as

$$C_\beta(S) = \frac{\iint_S (1 - \beta \cdot r/r_{\max}) dx dy}{\iint_{CH(S)} (1 - \beta \cdot r/r_{\max}) dx dy}. \quad (8)$$

Assume that  $S$  is scaled by a coefficient  $k$ , the convexity of the new shape in the new coordinate system is written as

$$\begin{aligned} C_\beta(S') &= \frac{\iint_{S'} (1 - \beta \cdot r'/r'_{\max}) dx' dy'}{\iint_{CH(S')} (1 - \beta \cdot r'/r'_{\max}) dx' dy'} \\ &= \frac{\iint_S (1 - \beta \cdot kr/kr_{\max}) k^2 dx dy}{\iint_{CH(S)} (1 - \beta \cdot kr/kr_{\max}) k^2 dx dy} \\ &= C_\beta(S), \end{aligned} \quad (9)$$

where the prime symbol indicates those corresponding parameters after scaling.  $\square$

### 3.3. Properties of the new convexity measure

Now we discover some new properties of  $C_\beta$  by showing its mathematical connections to  $C_4$ .

**Property 1.** For a given nonconvex planar shape  $S$ , letting  $\mu(D)$  and  $\mu(CH(S))$  be the average weights of its dents and convex hull, respectively, then

$$C_\beta(S) - C_4(S) \begin{cases} > 0, \text{ if } \mu(D) < \mu(CH(S)) \\ = 0, \text{ if } \mu(D) = \mu(CH(S)) \\ < 0, \text{ if } \mu(D) > \mu(CH(S)). \end{cases} \quad (10)$$

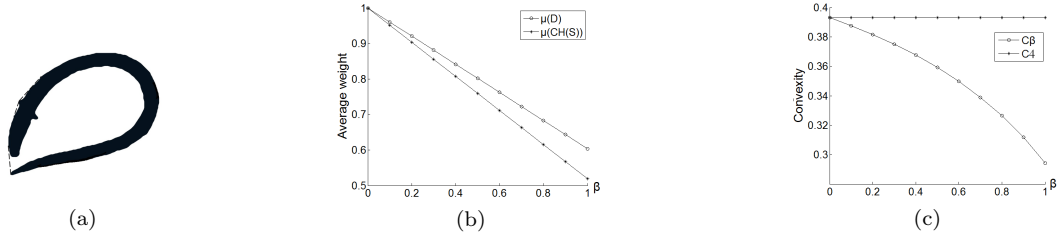


Figure 6: The dent in (a) embraces the GCCH of the shape. According to Properties 2 and 3, increasing  $\beta$  will enlarge the difference between  $\mu(D)$  and  $\mu(CH(S))$  and reduce the value of  $C_\beta$ .

*Proof.*

$$\begin{aligned}
C_\beta(S) - C_4(S) &= \frac{I(S)}{I(CH(S))} - \frac{Area(S)}{Area(CH(S))} \\
&= \frac{Area(D)}{Area(CH(S))} - \frac{I(D)}{I(CH(S))} \\
&= \frac{Area(D)}{Area(CH(S))} \cdot \left(1 - \frac{\mu(D)}{\mu(CH(S))}\right).
\end{aligned} \tag{11}$$

□

From Property 1 we can see that when dents are distant from the GCCH of  $S$ ,  $\mu(D)$  will be less than  $\mu(CH(S))$ , and the result of the new measure will be larger than  $C_4(S)$ . If dents are close to the GCCH,  $\mu(D)$  will be larger than  $\mu(CH(S))$ , and the result of the new measure will be less than  $C_4(S)$ . When  $\mu(D)$  is equal to  $\mu(CH(S))$ ,  $C_\beta(S)$  will be equal to  $C_4(S)$ .

**Property 2.** For a given nonconvex planar shape  $S$ , increasing  $\beta$  will enlarge the absolute difference between  $C_\beta(S)$  and  $C_4(S)$ .

*Proof.*

$$\begin{aligned}
|C_\beta(S) - C_4(S)| &= \left| \frac{Area(D)}{Area(CH(S))} - \frac{I(D)}{I(CH(S))} \right| \\
&= \left| \frac{Area(CH(S)) \iint_D \frac{\beta r}{r_{\max}} d\sigma - Area(D) \iint_{CH(S)} \frac{\beta r}{r_{\max}} d\sigma}{Area^2(CH(S)) - Area(CH(S)) \iint_{CH(S)} \frac{\beta r}{r_{\max}} d\sigma} \right|.
\end{aligned} \tag{12}$$

From Eq.(12) we can see that when  $\beta = 0$ ,  $C_\beta(S)$  and  $C_4(S)$  will be equal. When  $\beta > 0$ , the numerator and denominator of the equation can be divided by  $\beta$ , and then we can easily find that increasing  $\beta$  will enlarge the absolute difference between  $C_\beta(S)$  and  $C_4(S)$ :

$$\begin{aligned}
|C_\beta(S) - C_4(S)| &= \left| \frac{Area(CH(S)) \iint_D \frac{r}{r_{\max}} d\sigma - Area(D) \iint_{CH(S)} \frac{r}{r_{\max}} d\sigma}{\frac{1}{\beta} Area^2(CH(S)) - Area(CH(S)) \iint_{CH(S)} \frac{r}{r_{\max}} d\sigma} \right|.
\end{aligned} \tag{13}$$

□

Property 2 shows that if dents are distant from the GCCH of  $S$ , that is  $\mu(D) < \mu(CH(S))$ , increasing  $\beta$  will enlarge the value of  $C_\beta(S)$ . If dents are close to the GCCH, that is  $\mu(D) > \mu(CH(S))$ , increasing  $\beta$  will reduce the value of  $C_\beta(S)$ . When  $\beta$  decreases to 0,  $C_\beta$  will degenerate into  $C_4$ . The above cases are exemplified in Fig.5 and Fig.6. In practical applications, if we want to depress the influence of boundary noise, we can choose a large  $\beta$ . If there exist irregular non-noise boundaries, a small  $\beta$  may be adopted for better performance.



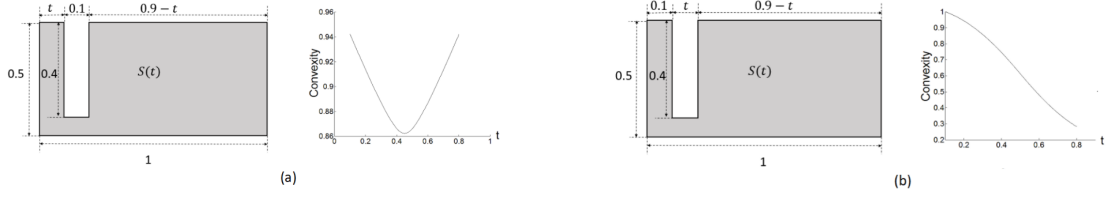


Figure 7: (a) When  $t$  changes from 0.1 to 0.8,  $C_\beta(S(t))$  monotonically decreases at first and then monotonically increases, as shown in the right graph of  $C_\beta(S(t))$  for  $t \in [0.1, 0.8]$ . (b) The gradual increase of  $t$  seems to hollow out  $S(t)$  and this explains the rationality of the descending of  $C_\beta(S(t))$ , as shown in the right graph of  $C_\beta(S(t))$  for  $t \in [0.0, 0.8]$ .

### 3.4. Implementation

For the implementation of  $C_\beta$ , we use a discrete version of Definition 7, where the integral symbols can be replaced by summations and discrete pixels in the image domain can be thought of as the infinitely small patches. Algorithm 1 shows the pseudocode of the new measure.

---

#### Algorithm 1 DWAI( $S, \beta$ )

---

**Input:** A shape,  $S$ , and a weighting parameter,  $\beta$ ;  
**Output:** Convexity value,  $C_\beta$ .  
1: compute the convex hull of  $S$ ,  $CH(S)$ ;  
2:  $N_{ch} \leftarrow$  the number of pixels in  $CH(S)$ ;  
3:  $N_s \leftarrow$  the number of pixels in  $S$ ;  
4: compute the position of the GCCH of  $CH(S)$ ;  
5: compute the Euclidean distances,  $r[N_{ch}]$ , between pixels in  $CH(S)$  and the GCCH, and the longest one is marked as  $r_{max}$ ;  
6: compute the weight of every pixel in  $CH(S)$ ,  $W[N_{ch}]$ ;  
7: **for**  $i = 1$  to  $N_{ch}$  **do**  
8:    $W[i] = 1 - \beta \cdot r[i]/r_{max}$ ;  
9: **end for**  
10: compute the influence of  $S$ ,  $I(S)$ ;  
11: **for** pixel,  $i \in S$  **do**  
12:    $I(S) += W[i]$ ;  
13: **end for**  
14: compute the influence of  $CH(S)$ ,  $I(CH(S))$ ;  
15: **for** pixel,  $i \in CH(S)$  **do**  
16:    $I(CH(S)) += W[i]$ ;  
17: **end for**  
18: **return**  $I(S)/I(CH(S))$ .

---

## 4. Comparisons

This section is dedicated to comparisons of the convexity measures mentioned in this paper on some representative shapes with their dents under affine transformations.

### 4.1. Comparisons with the area-based measures

Convexity values computed by  $C_4$  for shapes with an identical ratio of shape to convex hull areas but different dent depths are identical, as shown in Fig.3 (a) and (c). Instead the convexities of Shape (a), (b), and (c) in Fig.3 calculated by  $C_\beta$  are 0.9181, 0.8365, and 0.9398, respectively, which are in line with our human perception. It is worth noting that without specification, the parameter  $\beta$  is set to 1 by default in this paper.  $C_5$  is based on the MCS that considers the area difference between the shape and its maximum convex subset. Generally speaking, it is difficult to compute the MCS of an arbitrary shape and to justify its

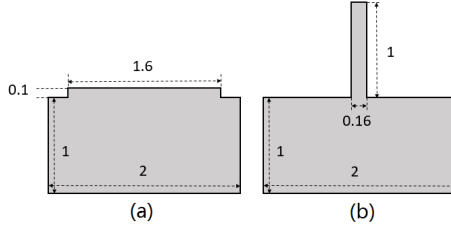


Figure 8: (a) and (b) have the same area and MCS, leading to the same  $C_5$  values, but (b) is apparently more concave than (a).

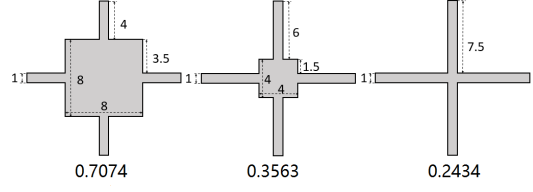


Figure 9: Convexities of the three shapes calculated by  $C_1$  are identical, 0.7250; the convexity values calculated by  $C_2$  are also the same, 0.5312. Therefore, they cannot sense the shrinking trend of the shapes. Underneath are their convexity values calculated by the new measure  $C_\beta$ .

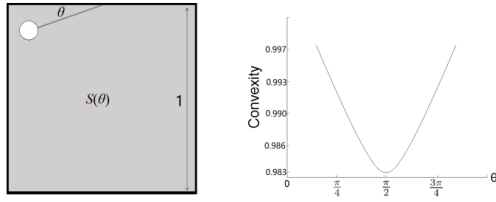


Figure 10: When increasing  $\theta$ , where  $\theta \in [\frac{\pi}{6}, \frac{5\pi}{6}]$ ,  $C_\beta(S(\theta))$  monotonically decreases at first and then monotonically increases. The diameter of the circular dent is 0.1. The length of the string linking the dent and the middle point of one  $t$  shape boundary is 0.35, and the string width is ignorable.

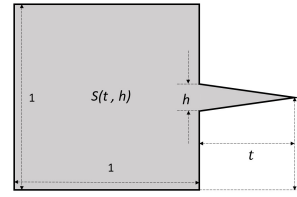


Figure 11: An unreasonable estimation by the probability-based measure  $C_\alpha$ , where  $\lim_{h \rightarrow 0} C_\alpha(S(t, h)) = 1$  for any fixed

convexity measurement results. Here a human crafted negative example is given in Fig.8, where the results calculated by  $C_5$  are identical and both equal to 0.9260, while the convexities calculated by  $C_\beta$  are 0.9973 and 0.6981. In Fig.7(a), the convexity becomes smaller when the dent approaches the GCCH. When the dent arrives at the GCCH, it imposes the maximum influence, and  $C_\beta(S(t))$  reaches the minimum value.  $C_5(S(t))$  has a similar performance. However, the values calculated by  $C_4(S(t))$  will not change.

#### 4.2. Comparisons with other convexity measures

In Fig.7(a),  $C_\alpha(S(t))$  has a similar performance to ours, while the values calculated by  $C_1(S(t))$  and  $C_2(S(t))$  will not change as  $t$  varies. Note that without specification,  $\alpha$  in  $C_\alpha$  is set to 0.5 by default, a value originally adopted in Rahtu et al. (2006).

As for Fig.7(b), the widening of  $t$  gives a sense that  $S(t)$  is being hollowed out. This can be verified by  $C_\beta(S(t))$ . However, neither  $C_1$  nor  $C_2$  senses this change and the convexity values calculated by them are invariable. Moreover, Fig.9 illustrates that  $C_1$  and  $C_2$  cannot distinguish the shapes in the figure, and this is, however, against the human perception that the convexity should decrease as the central square of the shape shrinks. This common sense can be verified by  $C_\beta$  instead.

Fig.10 illustrates that when  $\theta$  increases, the convexity calculated by  $C_\beta$  will first decrease and then increase. When  $\theta = \frac{\pi}{2}$ ,  $C_\beta$  will reach the minimum.  $C_\alpha$  has a similar performance, while  $C_2$  reaches the minimum when  $\theta = \frac{\pi}{4}$  or  $\theta = \frac{3\pi}{4}$ . However, the convexity values calculated by  $C_1$  and  $C_4$  are invariable.

The probability-based measure  $C_\alpha$  is insensitive to slim protrusions. For a given shape  $S(t, h)$  in Fig.11,  $\lim_{h \rightarrow 0} C_\alpha(S(t, h)) = 1$  for any fixed  $t$ , which is unreasonable anyway. This means, when the area of the protrusion approaches 0,  $C_\alpha(S(t, h))$  will be 1, regardless of the position and length of the protrusion. For a fixed  $t = 0.5$ , the results calculated by  $C_2$ ,  $C_4$ , and  $C_\beta$  for Fig.11 are 0.8, 0.8, and 0.8720, respectively. Moreover, convexity values computed by  $C_\alpha$  usually appear larger than expected, and this can be seen in the next section.













	1	2	3	4	5	6	7	8	9	10	11	12
												
$C_\beta$	1.0000	0.9529	0.8591	0.8545	0.8179	0.7949	0.7278	0.6820	0.5679	0.4723	0.3743	0.3311
$C_4$	1.0000	0.8936	0.8117	0.9017	0.7785	0.7336	0.5946	0.5562	0.5438	0.4264	0.3220	0.4986
$C_2$	1.0000	0.9100	0.5114	0.6986	0.4865	0.4706	0.3556	0.2918	0.4569	0.3612	0.5783	0.6153
$C_\alpha$	1.0000	0.9981	0.9441	0.8218	0.9189	0.9279	0.9047	0.9136	0.8402	0.6910	0.6500	0.5034

Figure 12: Shapes used for the quantitative evaluation.

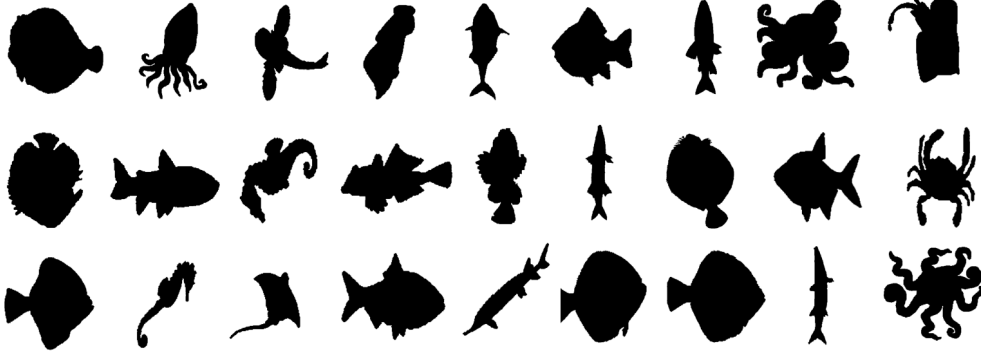


Figure 13: The shapes of various aquatics.

## 5. Experimental evaluations

In this section, we experimentally assess the performance of the convexity measures introduced in this paper, involving  $C_\beta$ ,  $C_2$ ,  $C_4$ , and  $C_\alpha$ , and identify characteristics of each measure. Note that  $C_5$  is excluded due to its computational difficulty while  $C_1$  and  $C_3$  are omitted in the experiments since they can be experimentally replaced by  $C_2$  [Zunic and Rosin \(2004\)](#) and  $C_\alpha$  [Rahtu et al. \(2006\)](#), respectively.

### 5.1. Quantitative comparison

We first perform a quantitative evaluation of different measures on a group of shapes shown in Fig.12. It can be seen that the convexity values computed by  $C_4$  and  $C_\beta$  are compliant with Property 1. Except Shape 4 and Shape 12, whose  $\mu(D) > \mu(CH(S))$ , all the nonconvex shapes have  $C_\beta$  larger than  $C_4$ , because their dents are relatively distant from their GCCHs, resulting in  $\mu(D) < \mu(CH(S))$ . Observing the convexity values of Shape 2 and Shape 4 calculated by  $C_2$  and  $C_\alpha$ , we find that they both consider that Shape 2 is more convex than Shape 4. However,  $C_4$  denies this fact. Although our measure stems from  $C_4$ , it can resolve this problem with the introduced DWAI. It can also be seen that  $C_2$  is too sensitive to downplay the impact of those tiny and slight dents as well as the edge noise. For instance, Shape 7 and Shape 8 are the two most concave shapes measured by  $C_2$  because the convexity calculated by  $C_2$  is determined by projecting the perimeter of the shape onto  $R(S, \varphi)$ . For Shape 3 and Shape 11, all the convexity measures consider that Shape 11 is much more concave than Shape 3 except  $C_2$ . It can be seen that all the convexity values computed by  $C_\alpha$  are greater than 0.5, and there are seven shapes whose convexity values are even greater than 0.9, which, however, cannot reflect the reality.

### 5.2. Robustness evaluation

In the second experiment, we test the robustness of the convexity measures in shape sorting with an increasing noise density. We use 27 aquatic shapes illustrated in Fig.13 for this experiment. First, we

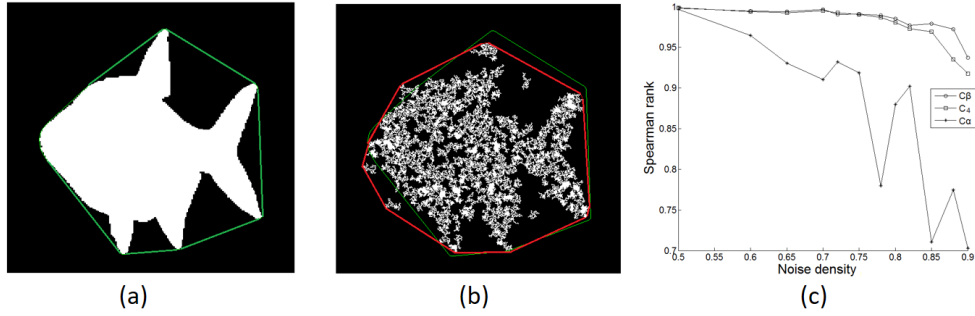


Figure 14: (a) Convex hull of the original aquatic shape in green. (b) Convex hull of the noisy shape in red. (c) Spearman rankings of using variant measures for the aquatic shapes with an increasing noise density. (For interpretation of the colors in the figure(s), the reader is referred to the web version of this article.)

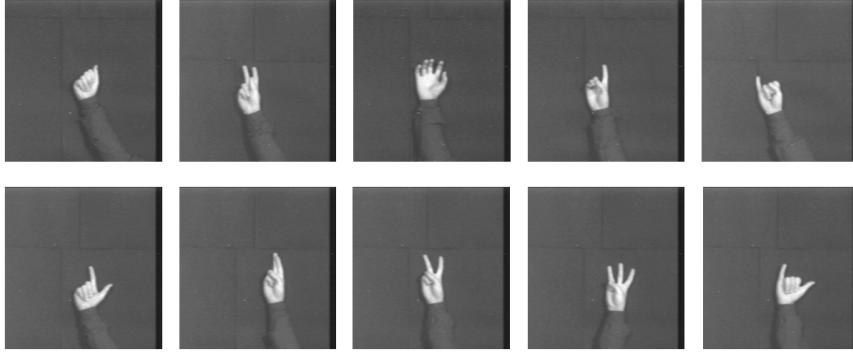


Figure 15: Samples of the 10 gesture categories.

compute the convexity values of the original aquatic shapes and sort them in order of convexity. Then we use salt and pepper noise with an increasing density to degrade the shapes. Fig.14(b) shows such a noisy aquatic shape with the noise density being 0.88. Next we compute the convexity values once more. After that we sort the noisy shapes in order of convexity and measure how this order is correlated with that of the original shapes. We use the convexity ranking data rather than the convexity values for estimating the correlation. In order to calculate the correlation between the two groups of shapes, we make use of the Spearman rank [Lehmann and D'Abrera \(2006\)](#) to estimate the correlation of two groups of data. As shown in Fig.14(c), both  $C_4$  and  $C_\beta$  perform far better than  $C_\alpha$ , demonstrating the robustness of the area-based measures against noise, and  $C_\beta$  beats  $C_4$  as the noise density increases further. As the noise density increases, some new dents and protrusions will be generated, which may change the convex hull of the shape, as shown in Fig.14(a) and (b). A slight change of the convex hull may impact on the convex hull based measures, such as  $C_4$ . However, the new measure can reduce the impact made by the convex hull change. Note that  $C_2$  is excluded in this experiment because when the noise density increases to a certain level, the shape may be separated apart, and the codes of  $C_2$  can no longer tolerate such a shape with more than one component.

### 5.3. Shape classification and retrieval

In the third experiment we apply the convexity measures to shape classification and retrieval with two datasets. The first dataset used is extracted from the Thomas Moeslund's Gesture Recognition Database, consisting of 10 categories with 820 gesture images. Some classified samples are shown in Fig.15. We first convert the input images into binary ones and then classify the binary images using different convexity

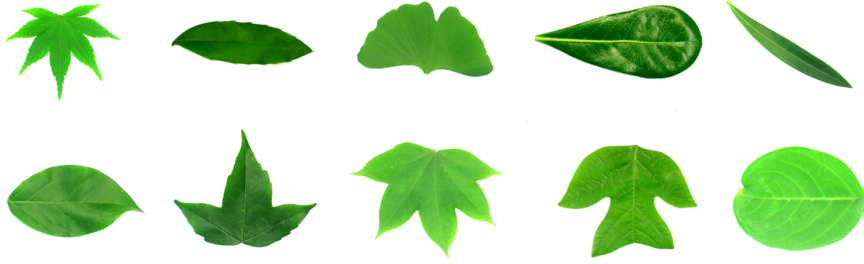


Figure 16: Samples of the 10 leaf categories.

Table 1: Results of correct classification percentages using different convexity measures.

Convexity measures	$C_{\beta=0.0}$	$C_{\beta=0.1}$	$C_{\beta=0.2}$	$C_{\beta=0.3}$	$C_{\beta=0.4}$	$C_{\beta=0.5}$
Hand gesture	69.4%	71.8%	76.5%	72.9%	74.1%	72.9%
Leaf	67.7%	67.7%	70.8%	70.2%	70.8%	69.6%
Convexity measures	$C_{\beta=0.6}$	$C_{\beta=0.7}$	$C_{\beta=0.8}$	$C_{\beta=0.9}$	$C_{\beta=1.0}$	$C_{\alpha=0.1}$
Hand gesture	68.2%	72.9%	<b>78.8%</b>	75.3%	65.9%	61.2%
Leaf	67.1%	<b>72.0%</b>	67.1%	65.8%	63.3%	57.1%
Convexity measures	$C_{\alpha=0.2}$	$C_{\alpha=0.3}$	$C_{\alpha=0.4}$	$C_{\alpha=0.5}$	$C_4$	$C_2$
Hand gesture	64.7%	71.8%	71.8%	71.8%	69.4%	62.4%
Leaf	49.7%	51.5%	52.8%	52.8%	67.7%	57.1%

measures. Classification is performed using the k-Nearest Neighbors classifier. In order to achieve a comprehensive assessment, the values of both  $\alpha$  and  $\beta$  are allowed to vary at regular intervals. Although  $0 < \alpha < 1$ , we need only to test a half range of  $C_\alpha$  due to its symmetry. As can be seen in Table 1,  $C_{\beta=0.8}$  achieves the best classification result. We also apply the convexity measures to shape retrieval. To help improve the retrieval precision, we enjoy the privilege that  $C_\beta$  can form different convexity measures by constructing a new shape descriptor CS (Convexity Statistics) with the mean, variance, skewness, and kurtosis of 5 different values of  $C_\beta$  with  $\beta = 0.6, 0.7, 0.8, 0.9, 1$  Zimmer et al. (2013). Impartially we also calculate the CS of five  $C_\alpha$ s with  $\alpha = 0.1, 0.2, 0.3, 0.4, 0.5$ . The retrieval performance is evaluated by four quantitative measures (NN, 1-Tier, 2-Tier, DCG) Shilane et al. (2004). The results are shown in Table 2. The second dataset tested in this experiment is extracted from the FLAVIA database Wu et al. (2007), consisting of 10 categories with 545 leaf images. Some classified samples are shown in Fig.16. The same classification and retrieval tests are carried out, the results of which are respectively shown in Table 1 and Table 2.

#### 5.4. Medical application

The importance of shape analysis in screening mammography has been frequently addressed in the literature. In the fourth experiment, we apply the convexity measures to classify 54 mammographic mass shapes selected from two well established mammogram databases, the MIAS and Screen Test databases Rangayya et al. (1997) as shown in Fig.17, and four classified examples of which are displayed in Fig.18. In this classification experiment, the nearest neighbor classifier is performed using the Euclidean distance. In order to produce statistically correct results the leave-one-out test is employed. We assess the measures by classifying them as malignant/benign and circumscribed/spiculated. The results are shown in Table 3. By varying the value of  $\beta$ ,  $C_{\beta=0}$  can achieve the same best classification rates as  $C_4$ . Moreover, from Table 3 we can also find a trend that the smaller the value of  $\beta$ , the higher the classification rate. This demonstrates what we have discovered previously, that is, for mass shapes with irregular boundaries a small  $\beta$  achieves better performance.

Table 2: Retrieval performance of the convexity measures and convexity statistics evaluated on the hand gesture and leaf datasets.

	Hand gesture				Leaf			
	NN	1-Tier	2-Tier	DCG	NN	1-Tier	2-Tier	DCG
$CS$ for $C_\beta$	<b>85.1%</b>	<b>69.9%</b>	<b>86.2%</b>	<b>90.4%</b>	<b>77.6%</b>	<b>65.4%</b>	<b>82.5%</b>	<b>88.0%</b>
$CS$ for $C_\alpha$	81.6%	46.7%	64.2%	82.7%	51.7%	30.6%	53.3%	70.8%
$C_4$	61.3%	58.2%	79.0%	83.1%	58.2%	54.3%	77.6%	81.1%
$C_2$	48.5%	45.8%	70.5%	78.1%	53.6%	47.1%	71.4%	76.4%

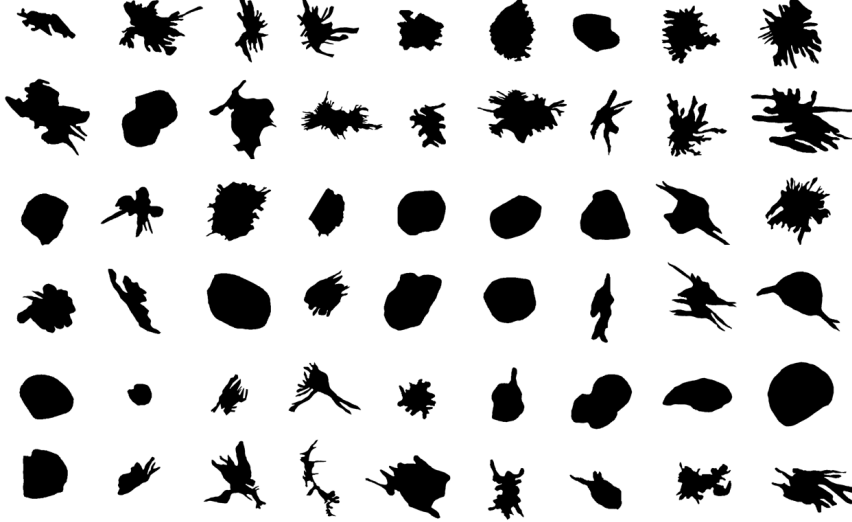


Figure 17: The 54 mammographic mass shapes

## 6. Limitation

Although the new measure can resolve most problems of  $C_4$ , it also shares a problem with  $C_4$ , as the new measure is derived from  $C_4$ . In Fig.11, when  $t \rightarrow \infty$ , the values calculated by  $C_\beta$  and  $C_4$  both approach 0, which are unreasonable. As  $t \rightarrow \infty$ , the dominant part of  $S(t, h)$  is the protrusion, which is convex. The results of  $C_1$ ,  $C_2$ ,  $C_3$ ,  $C_5$ , and  $C_\alpha$  are 1, which are relatively more reasonable.

## 7. Conclusions

For the first time we have developed a new area-based convexity measure to improve  $C_4$ , making the most commonly used convexity measure fully replaceable. By turning the convexity measurement into a problem of influence evaluation through the DWAI, the new measure resolves the major problems of  $C_4$  and, as an area-based measure, outperforms the mainstream competitors in many aspects. The examples and experiments in the paper have also demonstrated the discovery that the attributes of dents, such as the position, area, and depth with respect to the GCCH of the shape, dominate the convexity measurement. Although we believe this idea is more reasonable than the existing hypotheses in convexity measurement, a study or proof from cognitive or psychological point of view is still welcome in the future.

Moreover, similar to  $C_\alpha$ ,  $C_\beta$  enables the area-based measure to construct a variety of convexity measures by varying the value of  $\beta$  which, however, offers a great advantage over  $C_4$  in practical applications. Our measure also leaves a large degree of freedom for further exploration. For example, this paper only considers the DWAI, a derivative of WAI, but we believe the form of the WAI would be versatile enough to be explored in the future.

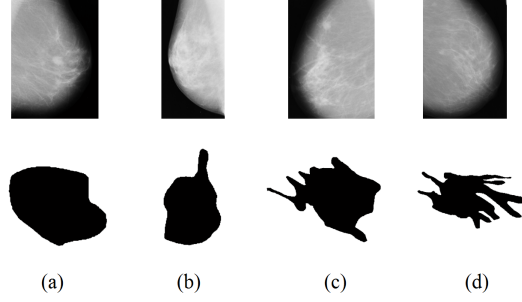


Figure 18: Four classified examples of the mammographic masses: Benign (Shape (a) and (c)), Malignant (Shape (b) and (d)), Circumscribed (Shape (a) and (b)), Spiculated (Shape (c) and (d)). The masses are extracted from the mammograms in the first row and rescaled for the sake of visibility.

Table 3: Results of correct classification percentages using different convexity measures for mammographic masses.

Convexity measures	$C_{\beta=0.0}$	$C_{\beta=0.1}$	$C_{\beta=0.2}$	$C_{\beta=0.3}$	$C_{\beta=0.4}$	$C_{\beta=0.5}$
Mal./ben.	<b>68.52%</b>	66.67%	66.67%	62.96%	62.96%	62.96%
Circ./spic.	<b>90.74%</b>	<b>90.74%</b>	<b>90.74%</b>	<b>90.74%</b>	87.04%	85.19%
Convexity measures	$C_{\beta=0.6}$	$C_{\beta=0.7}$	$C_{\beta=0.8}$	$C_{\beta=0.9}$	$C_{\beta=1.0}$	$C_{\alpha=0.1}$
Mal./ben.	62.96%	64.81%	62.96%	62.96%	62.96%	64.81%
Circ./spic.	85.19%	85.19%	85.19%	87.04%	85.19%	83.33%
Convexity measures	$C_{\alpha=0.2}$	$C_{\alpha=0.3}$	$C_{\alpha=0.4}$	$C_{\alpha=0.5}$	$C_4$	$C_2$
Mal./ben.	57.41%	62.96%	66.67%	66.67%	<b>68.52%</b>	61.11%
Circ./spic.	<b>90.74%</b>	88.89%	85.19%	87.04%	<b>90.74%</b>	81.48%

In this paper the newly proposed convexity measure has been experimentally demonstrated in shape classification and retrieval. In fact, there are more potential research areas which may benefit from the new convexity measure. For example, a routine of shape decomposition is to divide a given polygon into approximate convex components according to shape concavity [Lien and Amato \(2006, 2007\)](#). Nevertheless, concavity neither has a well-accepted definition, nor is independent of polygon size [Lien and Amato \(2006\)](#). Therefore, our convexity measure provides a possible solution to these problems.

We only consider 2D convexity measures for planar shapes. It is, however, straightforward to extend this idea of influence evaluation to 3D shape analysis. We believe this will benefit the relevant research fields further.

## 8. Acknowledgements

The authors would like to sincerely thank Professor Rosin for sharing his codes and datasets. This work was supported by the Open Research Fund of Shanghai Key Laboratory of Multidimensional Information Processing, East China Normal University.

## References

- Asafi, S., Goren, A., Cohen-Or, D., 2013. Weak convex decomposition by lines-of-sight. *Computer Graphics Forum* 32, 23–31.
- Attene, M., Mortara, M., Spagnuolo, M., Falcidieno, B., 2008. Hierarchical convex approximation of 3D shapes for fast region selection. *Computer Graphics Forum* 27, 1323–1332.
- Bribiesca, E., 2008. An easy measure of compactness for 2D and 3D shapes. *Pattern Recognition* 41, 543–554.
- Ghosh, M., Amato, N.M., Lu, Y., Lien, J.M., 2013. Fast approximate convex decomposition using relative concavity. *Computer-Aided Design* 45, 494–504.
- Lehmann, E.L., D’Abrera, H.J., 2006. *Nonparametrics: Statistical methods based on ranks*. Springer New York.
- Li, R., Liu, L., Sheng, Y., Zhang, G., 2017. A heuristic convexity measure for 3D meshes. *The Visual Computer* 33, 903–912.

- Lian, Z., Godil, A., Rosin, P.L., Sun, X., 2012. A new convexity measurement for 3D meshes, in: CVPR, IEEE. pp. 119–126.
- Lian, Z., Rosin, P.L., Sun, X., 2010. Rectilinearity of 3D meshes. *International Journal of Computer Vision* 89, 130–151.
- Lien, J.M., Amato, N.M., 2006. Approximate convex decomposition of polygons. *Computational Geometry* 35, 100–123.
- Lien, J.M., Amato, N.M., 2007. Approximate convex decomposition of polyhedra, in: *Proceedings of the 2007 ACM symposium on Solid and physical modeling*, ACM. pp. 121–131.
- Liu, H., Liu, W., Latecki, L.J., 2010. Convex shape decomposition, in: CVPR, IEEE. pp. 97–104.
- Loncaric, S., 1998. A survey of shape analysis techniques. *Pattern recognition* 31, 983–1001.
- Pao, H., Geiger, D., Robin, N., 1999. Measuring convexity for figure/ground separation, in: ICCV, IEEE. pp. 948–955.
- Proffitt, D., 1982. The measurement of circularity and ellipticity on a digital grid. *Pattern Recognition* 15, 383–387.
- Rahtu, E., Salo, M., Heikkilä, J., 2006. A new convexity measure based on a probabilistic interpretation of images. *Pattern Analysis and Machine Intelligence, IEEE Transactions on* 28, 1501–1512.
- Rangayya, R.M., Elfaramawy, N.M., Desautels, J.E., Alim, O.A., 1997. Measures of acutance and shape for classification of breast tumors. *Medical Imaging, IEEE Transactions on* 16, 799–810.
- Rosin, P., 2009. Classification of pathological shapes using convexity measures. *Pattern Recognition Letters* 30, 570–578.
- Rosin, P.L., 1999. Measuring rectangularity. *Machine Vision and Applications* 11, 191–196.
- Rosin, P.L., 2003. Measuring shape: Ellipticity, rectangularity, and triangularity. *Machine Vision and Applications* 14, 172–184.
- Rosin, P.L., Mumford, C.L., 2006. A symmetric convexity measure. *Computer Vision and Image Understanding* 103, 101–111.
- Rosin, P.L., Zunic, J., 2007. Probabilistic convexity measure. *IET Image Processing* 1, 182–188.
- Shilane, P., Min, P., Kazhdan, M., Funkhouser, T., 2004. The Princeton shape benchmark, in: *Shape Modeling International*, pp. 167–178.
- Song, Y., Pickup, D., Li, C., Rosin, P., Hall, P., 2013. Abstract art by shape classification. *Visualization and Computer Graphics, IEEE Transactions on* 19, 1252–1263.
- Wu, S.G., Bao, F.S., Xu, E.Y., Wang, Y.X., Chang, Y.F., Xiang, Q.L., 2007. A leaf recognition algorithm for plant classification using probabilistic neural network, in: *IEEE International Symposium on Signal Processing and Information Technology*, pp. 11–16.
- Zhou, R., Yuan, J., Liu, W., 2013. Minimum near-convex shape decomposition. *Pattern Analysis and Machine Intelligence, IEEE Transactions on* 35, 2546–2552.
- Zimmer, H., Campen, M., Kobbelt, L., 2013. Efficient computation of shortest path-concavity for 3d meshes, in: CVPR, IEEE. pp. 2155–2162.
- Zunic, J., Hirota, K., Rosin, P.L., 2010. A Hu moment invariant as a shape circularity measure. *Pattern Recognition* 43, 47–57.
- Zunic, J., Rosin, P.L., 2003. Rectilinearity measurements for polygons. *Pattern Analysis and Machine Intelligence, IEEE Transactions on* 25, 1193–1200.
- Zunic, J., Rosin, P.L., 2004. A new convexity measure for polygons. *Pattern Analysis and Machine Intelligence, IEEE Transactions on* 26, 923–934.